Factors controlling the incubation in the application of ps laser pulses on copper and iron surfaces

B. Neuenschwander*[a], B. Jaeggi[a], M. Schmid[a], A. Dommann[b], A. Neels[b], T. Bandi[b], G. Hennig[c]

[a]Bern University of Applied Sciences, Institute for Applied Laser, Photonics and Surface Technologies ALPS, Pestalozzistrasse 20, 3400 Burgdorf, Switzerland

[b]CSEM, Microsystems Technology, Jaquet-Droz 1, 2002 Neuchatel, Switzerland

[c]Daetwyler Graphics, Flugplatz, 3368 Bleienbach, Switzerland

ABSTRACT

For laser micro processing with short and ultra-short pulses the threshold fluence is affected by the incubation and changes with the number of pulses applied. In general the incubation effect is described by a power function including the incubation coefficient *S*. Beside the threshold fluence also the energy penetration depth is subject to the incubation effect; moreover it is a main cause for the change of the threshold fluence with increasing pulse number.

The behavior of the threshold fluence can be explained by varying absorption (due to changes in the surface reflectivity), chemical changes of the surface (e.g. due to oxidation) or changes in the microstructure of the material whereas the behavior of the energy penetration depth could be explained by the latter two effects but should not be affected by a change in the absorption. To try to distinguish between these three effects a systematic ablation study with 10 ps pulses at 1064nm wavelength on copper and iron under different gases atmospheres and pressures was done.

The results show on the one hand the change of the energy penetration depth is the main cause of the incubation and that on the other hand an adapted model better fits the trend of the threshold fluence and the penetration depth as a function of the number of pulses applied. The influence of the gas (air, oxygen, nitrogen and argon) is only marginal whereas a reduction of the pressure from normal atmosphere down to 50 mbar results in a 25% increase of the maximum removal rate. Induced changes in the microstructure were detected by a high resolution X-ray diffraction analysis on single crystal (111-orientation) copper and iron samples.

Keywords: ultra-short pulses, incubation, threshold fluence, energy penetration depth, x-ray diffraction analysis

1. INTRODUCTION

For laser micro processing with ultra-short pulses the threshold fluence denotes one of the most important and reported parameter as it defines the minimum pulse energy which is needed for the ablation process. For metals the threshold fluence is almost constant for pulse durations from fs up to about 10 ps[1-4] and slightly increases for longer pulses[5]. Further many materials show an incubation effect i.e. the threshold fluence also depends on the number of pulses applied which was first in detail described for metals and ns-pulses in[6]. The authors propose to describe the incubation effect for the threshold fluence ϕ_{th} by a power function

$$\phi_{th}(N) = \phi_1 \cdot N^{S-1} \qquad (1)$$

With ϕ_1 the single shot threshold and *S* the incubation coefficient. In general the value of the threshold fluence decreases when the number of pulses is increased i.e. $S<1$ holds. In this work the incubation is related to the storage cycle of

*beat.neuenschwander@bfh.ch; phone +41 34 426 42 20; fax +41 34 423 15 13; laserlab.ti.bfh.ch

thermal stress-strain energy i.e. accumulation of plastic deformations[7] induced by the laser pulses. $S<1$ means that the material gets softer with increasing pulse number whereas for $S>1$ the material would become harder. This model fits the deduced threshold fluences quite well and was also confirmed (with $S>1$) for ultra-short pulses in the fs regime for metals[8-10], semiconductors[11] and transparent materials[12,13]. In this regime it is not clear if the explanation with the thermal stress-strain energy[6] is still applicable. Increased absorption arising from a rougher surface due to formed ripples[14] is an alternative approach to explain the nature of the incubation.

Expression (1) implies that for an infinite high number of pulses the threshold fluence should converge to zero which is not physical. Therefore an alternative model with an exponential drop and an offset representing the constant threshold fluence for an infinite number of pulses is proposed for fused silica and CaF_2 and LiF[11] but it does not fit better the values obtained for metals[3]. Additionally, in general the energy penetration depth δ is not included in the analysis of the incubation effect but this parameter is of great importance as it defines the maximum obtainable material removal rate[15] together with the threshold fluence. It has been found that also the energy penetration depth is a subject to incubation as well and that its behavior follows the threshold fluence[3,4]. Taking this into account the nature of incubation becomes important because a single variation of the absorption or reflection without influence onto the material only should affect the threshold fluence whereas material changes like surface oxidation, plastic deformations etc. should affect the energy penetration depth, as well.

2. THEORY

For ultra-short pulses the heat-transfer process in metals is described with the two temperature model[1,2,16-19] where the temperatures of the electrons and the lattice are treated separately. The results of the model and the experiments show, that the ablation depth z_{abl} can be written as a function of the applied fluence ϕ (pulse energy per unit area):

$$z_{abl} = \delta \cdot \ln\left(\frac{\phi}{\phi_{th}}\right) \tag{2}$$

with ϕ_{th} the threshold fluence and δ the energy penetration depth. Frequently two different ablation regimes are reported[2,20]: firstly the low fluence regime where the optical penetration depth dominates and secondly the high fluence regime where the energy transport is dominated by the heat diffusion of the hot electrons. The two regimes show different threshold fluences and penetration depths whereupon the corresponding values for the second regime are higher.

This logarithmic ablation law is a consequence of an exponential drop of the energy flux $F(z)$ in the material with the distance z to the interface.

$$F(z) = F_0 \cdot e^{-\frac{z}{\delta}} \tag{3}$$

At the interface the incident energy flux F_0 is directly scaled with the applied fluence via

$$F_0 = A \cdot \phi = (1-R) \cdot \phi \tag{4}$$

The energy per unit area, deposited in the material, directly scales with the first derivative of the flux with respect to z.

$$\frac{dE}{dV}(z) = \frac{1}{\delta} \cdot F(z) = \frac{1}{\delta} \cdot F_0 \cdot e^{-\frac{z}{\delta}} \tag{5}$$

All material is ablated up to a depth where the absorbed energy per unit volume corresponds to

$$\left.\frac{dE}{dV}\right|_{\min} = \rho \cdot \Omega_{vap} \tag{6}$$

with ρ the density and Ω_{vap} specific heat of evaporation. Typical values for $\rho \cdot \Omega_{vap}$ are summarized in Table 1. Under the assumption that the lateral energy transfer can be neglected and that the material begins to evaporate after the energy is deposited, (2) can be deduced by introducing (6) into (5) and taking account of (4). The threshold fluence can then be expressed by the surface reflectivity R, the energy penetration depth δ, and the material parameters ρ and Ω_{vap}:

$$\phi_{th} = \frac{\delta}{1-R} \cdot \rho \cdot \Omega_{vap} \tag{7}$$

This clearly shows that the threshold fluence directly scales with the penetration depth. For 10ps pulses and wavelengths around 1 µm the first ablation regime was not observed for copper and iron and was only weak for aluminum i.e. the energy transport is dominated by the electron diffusion. For pulses down to 250 fs an acceptable throughput is only achieved in the second ablation regime with the values of δ far above the optical penetration depth[3,4] i.e. the penetration depth δ should be measured and can't automatically be assumed as the optical one, even in the regime of fs-pulses.

Table 1. Energy per unit volume for evaporation

	Cu	Al	Fe	Au	Ag	W	Pt
$\rho \cdot \Omega_{vap}$ / $10^9 J/m^3$	44.2	29.5	51.3	31.9	25.1	81.9	57.0

If both parameters, ϕ_{th} and δ, are subject to incubation and assuming that the material parameters ρ and Ω_{vap} do not change, one is able to distinguish between the part which is caused by the change of the penetration depth and the part which is caused by the change in the reflectivity due to surface variations as e.g. ripples:

$$1-R(N) = \frac{\delta(N)}{\phi_{th}(N)} \cdot \rho \cdot \Omega_{vap} \tag{8}$$

In addition also the maximum obtainable removal rate is given by the two parameters and may therefore also depend on the number of pulses applied. The maximum removal rate for a Gaussian beam is given by[3,4,15]:

$$\frac{\dot{V}_{\max}(N)}{P_{av}} = \frac{2}{e^2} \cdot \frac{\delta(N)}{\phi_{th}(N)} = \frac{2}{e^2} \cdot \frac{1-R(N)}{\rho \cdot \Omega_{vap}} \tag{9}$$

For doing this the threshold fluence as well as the penetration depth has to be measured as a function of the number of pulses applied.

3. EXPERIMENTAL SET-UP

The experiments were performed with a DUETTO™ (Time Bandwidth Products, Switzerland) ps-laser system working at a wavelength of 1064 *nm* with pulse duration of about 10 *ps*. The system included an additional picker after the last amplifier stage as a pulse on demand (POD) option to be able to reduce the repetition rate down to single pulses. The control of the pulse energy going with the average power was done after the last amplifier stage with polarizer and λ/2-plates to guarantee constant beam parameters. The linear polarized beam was guided via folding mirrors through a beam expander into a galvo scanning head where it was focused by an f = 160 mm f-theta objective onto the target. The beam quality and spot size was measured with a rotating slit beam profiler, the corresponding values were w_0 = 17.8 µm and M^2 = 1.2.

The target was placed into a process chamber which could be evacuated down to 50 mbar and permanently flooded with O_2, N_2 or Ar as process gases. The target was placed in the focal plane of the lens which was deduced with the glass lid on the chamber. As targets copper (Cu-DHP and (111) single crystal), pure iron (sheets and (111) single crystal) and Aluminum sheets were used. To guarantee constant surface quality the sheet samples were polished in multiple steps, finally with a 3 µm diamond suspension. The surfaces of the single crystals were polished (electro polishing is assumed) by the supplier.

In order to deduce ϕ_{th} and δ as a function of the number of pulses applied, series with single ablated craters were generated for N = 1,2,4,...,512 pulses. For one series the pulse energy was raised from below up to multiples of the threshold. To avoid thermal accumulation effects the repetition rate was set to 50 *Hz* or less with the POD. The crater depths in the center were deduced with a confocal laser scanning microscope. Especially at low pulse energies i.e. low fluences or low number of pulses the deduction of the crater depth became extensive and sometimes almost impossible. On the other side, high fluences and pulse numbers lead to deep craters where it was no longer possible to measure the depth in the center.

The measured depths for a given number of pulses N were compared with the theoretical crater depth by introducing the peak fluence into (2). The two parameters $\phi_{th,N}$ and δ_N were then deduced by a least square fit to the experimentally obtained data. With a jackknife algorithm the standard deviations for $s_{\phi,N}$ and $s_{\delta,N}$ were calculated. If a model e.g. (1) for the incubation is known, these deviations together with the deduced values $\phi_{th,N}$ and δ_N formed the base for a Monte Carlo simulation to deduce the deviation of the model parameters e.g. ϕ_1 and S_ϕ for (1). Such an analysis was performed for Cu-DHP, aluminum and iron under air for Cu-DHP (with normal pressure, 500 mbar and 50 mbar) for aluminum and iron (normal pressure and outside of the process chamber). For copper additionally the influence of the process gases Ar, O_2 and N_2 at a pressure of 500 mbar was investigated.

The two (111) single crystals (Cu and Fe) were treated under air with normal pressure, 500 mbar, 250 mbar and 50 mbar and were only used for an X-ray diffraction analysis (at CSEM) to visualize local defects in the crystal lattice introduced by laser pulses.

4. RESULTS

4.1 Incubation Model

Figure 1 shows the deduced threshold fluence and energy penetration depth as a function of the number of pulses applied. It can clearly be seen that both parameters are strongly affected by the incubation. Similar behavior is obtained for all other investigated metals, gases and pressures. The dashed black line indicates the fit with the standard model (power function) according to (2). As it can be seen this model especially does not fit the measured values a low pulse numbers, therefore this model was supplemented with a constant offset i.e. the threshold value and the penetration depth at infinite number of pulses:

$$\phi_{th}(N) = \phi_{th,0} + \Delta\phi_{th} \cdot N^{n_\phi} \quad and \quad \delta(N) = \delta_0 + \Delta\delta \cdot N^{n_\delta} \tag{10}$$

The red lines in fig. 1 represent the according least square fits. This alternative model now fits better the values at low pulse numbers and is still accurate for high number of pulses. The similar behavior between the two models is also observed for all other situations. However, compared to the equation (10) the model represented by the equation (2) is simpler and allows analytical calculations e.g. of equation (8).

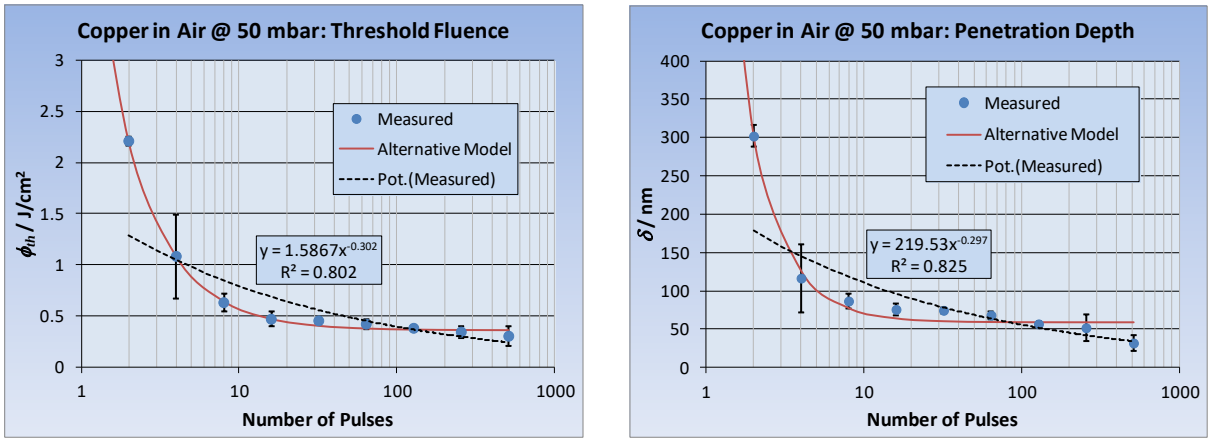

Figure 1. Threshold fluence and penetration depth as a function of the number of pulses applied for copper in air and a pressure of 50 mbar. The error bars indicate 3 times the standard deviation obtained from the jackknife analysis. The dashed line represents the fit with a power function whereas the red soli line is the fit with the alternative model.

The mean values and standard deviations of the model parameters $\phi_{th,1}$, S_ϕ, δ_1, S_δ and $\phi_{th,0}$, $\Delta\phi_{th}$, n_ϕ, δ_0. $\Delta\delta$, n_δ were deduced by a Monte-Carlo simulation and the results are summarized in table 2 for the standard model (2) and table 3 for the alternative model (10).

The deviations for the standard model are of 10% magnitude whereas for the alternative model these deviations are higher especially for the second and the third parameter. Note that $\phi_{th,0}+\Delta\phi_{th}$ and $\delta_0+\Delta\delta$ denote the corresponding single pulse values. Whether the deviations for these values are quite high, the error significantly drops for higher pulse numbers e.g. for aluminum under normal conditions and 1 pulse the Monte Carlo simulation for the alternative model

predicts $\phi_{th,1}$=3.85J/cm^2±1.20 J/cm^2 and δ_1=635nm±315nm whereas the values are ϕ_{th}=0.288J/cm^2±0.024 J/cm^2 and δ=55.8nm±6.0nm for 16 pulses respectively ϕ_{th}=0.159J/cm^2±0.014J/cm^2 and δ_1=35.6nm±5.05nm for 256 pulses.

Table 2: Standard model (2) parameters with its standard deviations.

Material	Gas	p / mbar	$\phi_{th,1}$ / J/cm^2	S_ϕ	δ_1 / nm	S_δ
Cu	Air	1000	1.71 ± 0.14	0.698 ± 0.019	149 ± 18.2	0.764 ± 0.029
Cu	Air	500	1.55 ± 0.25	0.671 ± 0.043	164 ± 30.1	0.724 ± 0.048
Cu	Air	50	1.58 ± 0.12	0.699 ± 0.019	223 ± 39.5	0.698 ± 0.070
Cu	Ar	500	1.72 ± 0.19	0.671 ± 0.024	199 ± 29.7	0.708 ± 0.034
Cu	N_2	500	1.88 ± 0.15	0.663 ± 0.020	195 ± 16.3	0.698 ± 019
Cu	O_2	500	2.05 ± 0.11	0.637 ± 0.016	282 ± 13.8	0.615 ± 0.014
Fe	Air	1000	0.16 ± 0.020	0.788 ± 0.020	45.9 ± 2.52	0.642 ± 0.011
Al	Air	1000	1.93 ± 0.17	0.504 ± 0.021	338 ± 41.6	0.500 ± 0.028

Table 3: Alternative model (9) parameters with its standard deviations.

Material	Gas	p / mbar	$\phi_{th,0}$ / J/cm^2	$\Delta\phi_{th}$ / J/cm^2	n_ϕ	δ_0 / nm	$\Delta\delta$ / nm	n_δ
Cu	Air	1000	0.33 ± 0.03	3.78 ± 1.1	1.026 ± 0.22	41.1 ± 6.13	273 ± 114	0.913 ± 0.32
Cu	Air	500	0.25 ± 0.03	2.29 ± 0.27	0.786 ± 0.10	33.5 ± 5.14	192 ± 26	0.637 ± 0.12
Cu	Air	50	0.36 ± 0.02	5.01 ± 1.54	1.380 ± 0.27	57.9 ± 10.5	951 ± 390	1.882 ± 0.49
Cu	Ar	500	0.32 ± 0.04	5.11 ± 1.61	1.29 ± 0.38	50.0 ± 4.86	756 ± 398	1.603 ± 0.56
Cu	N_2	500	0.33 ± 0.04	4.22 ± 1.19	1.078 ± 0.23	47.4 ± 4.40	479 ± 195	1.322 ± 0.39
Cu	O_2	500	0.31 ± 0.02	6.37 ± 0.73	1.223 ± 0.09	48.0 ± 1.26	2140 ± 346	2.172 ± 0.18
Fe	Air	1000	0.05 ± 0.004	11.74 ± 6.42	2.817 ± 0.38	7.37 ± 0.26	243 ± 87.3	1.533 ± 0.15
Al	Air	1000	0.15 ± 0.018	3.68 ± 1.16	1.186 ± 0.21	34.5 ± 7.26	616 ± 324	1.221 ± 0.41

Following the standard model the obtained single pulse threshold for copper in air amounts 1.71J/cm^2±0.14J/cm^2 which is in a very good agreement with the value of 1.7J/cm^2±0.3J/cm^2 reported by Byskov-Nielsen[10] but the incubation coefficient S_ϕ = 0.7±0.02 differs from the reported 0.85±0.03. In contrast the alternative model would predict a much higher value for the single pulse threshold of 4.11J/cm^2±1.13J/cm^2. Additional accurate measurements at low number of pulses should be done to finally evaluate the two models. As the alternative model also fits better the values up to 16 or 32 pulses it will be used here keeping in mind that values for less than 10 pulses may be very inaccurate.

From all presented measurements it can clearly be seen that the incubation effect is strong also for the energy penetration depth δ i.e. that according to (7) the incubation for the threshold fluence is mainly driven by the variation of the energy penetration depth.

4.2 Influence surrounding pressure

Fig. 3 shows on the left side the deduced maximum removal rates for Cu-DHP in air for three different pressures. As expected the results are inconsistent due to the high errors for low pulse numbers but from 32 pulses on the removal rate clearly increases when the pressure is decreased. Compared to normal atmosphere condition an increase of about 25% can be achieved for a pressure of 50 mbar. This increase could be caused by a reduced specific heat of evaporation Ω_{vap}.

On the right side of fig. 2 microscope pictures of the ablated craters are shown. The number of pulses is increased (1,2,4,8, .. 512) from right to the left and the fluence is decreased top down. The targets are not cleaned and the small cords are due to the cotton pads wherein the Cu-DHP sheet was placed for storage. Higher debris around the craters is observed for lower pressures which correspond to the higher removal rate. Fig. 3 shows SEM pictures of the ablated craters at a peak fluence of 1.82 J/cm^2 for 2 and 128 pulses. For 2 pulses almost no difference can be observed. With 128 pulses the crater is surrounded by a ring with low debris. For normal pressure ripples with melted and sintered debris are

observed. These ripples are still present but less pronounced at a pressure of 500 mbar and almost vanish at 50 mbar. At lower pressure the crater seems to be deeper than the other two.

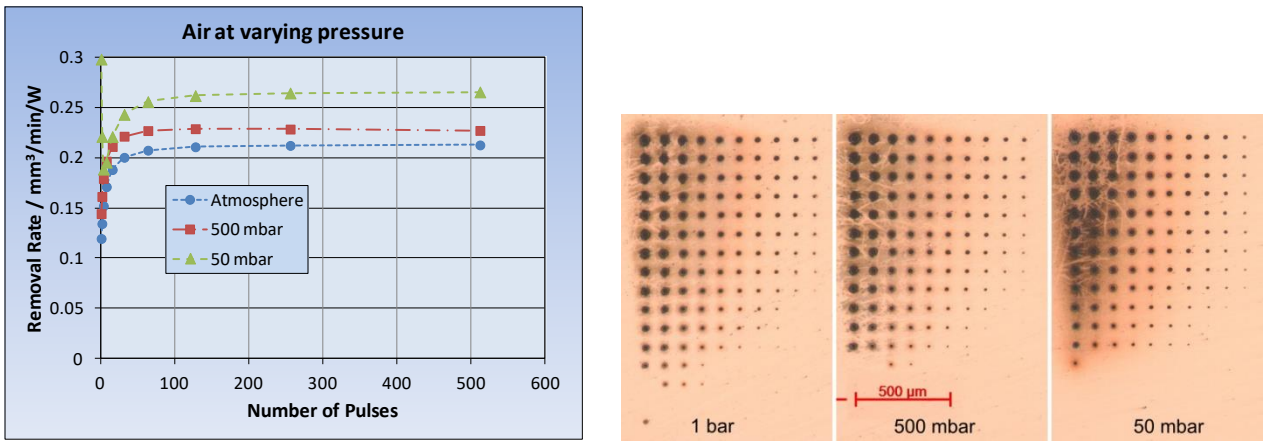

Figure 2. Left: Maximum removal rate for Cu-DHP calculated with the alternative model for 3 different pressures and air. Right: Ablated craters with raised pulse number from right to the left and decreased fluence top to down.

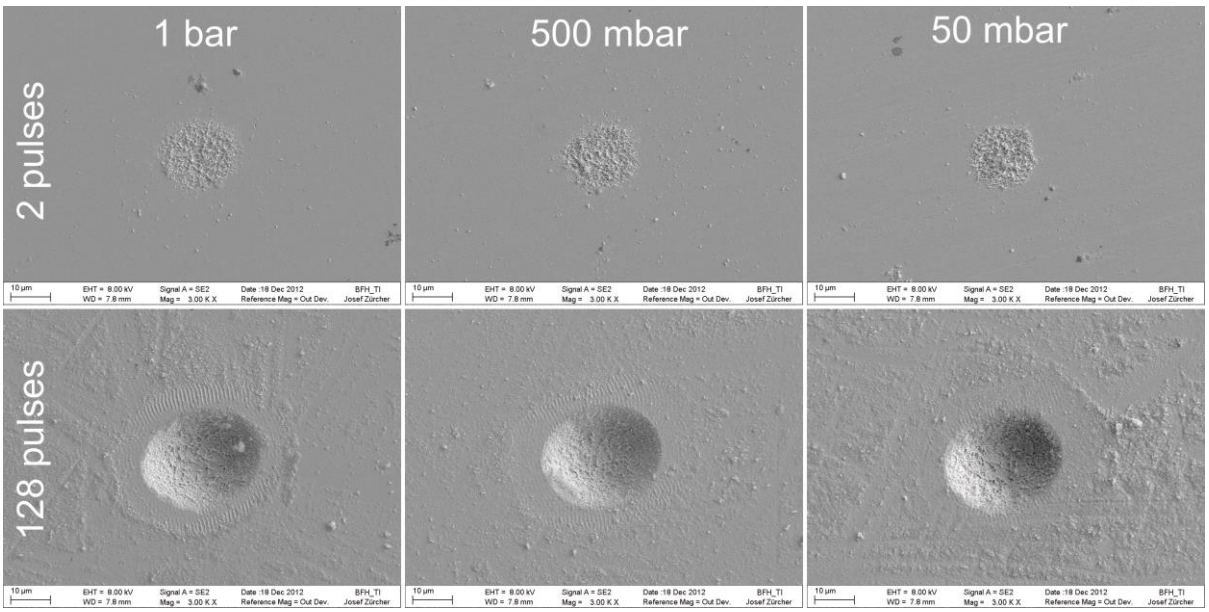

Figure 3. SEM pictures of ablated craters in Cu-DHP with 2 and 128 pulses at a peak fluence of 1.82 J/cm^2 in air at three different pressures.

4.3 Influence of the process gas

The ablation study on Cu-DHP was also performed for air, argon, nitrogen and oxygen at a pressure of 500 mbar to study the influence of the process gas. The maximum removal rate is shown in the left part of Fig. 4. For higher pulse numbers a small difference of about 10% can be observed between argon/oxygen and air/nitrogen. In contrast huge differences are observed on the pictures from the optic microscope (fig. 4 right). Most debris is found for argon, followed by nitrogen but almost no difference between oxygen and air can be observed. It is assumed that argon and nitrogen, often used as shielding gases, do prevent from oxidation and burning of the ablated particles which finally must lead to higher debris.

SEM pictures of ablated craters ablated with 2 and 128 pulses at peak fluences of 1.82 J/cm^2 an 3.0 J/cm^2 are shown in fig. 5. For two pulses there is no significant difference between the different process gases whereas huge differences can be observed with 128 pulses. For air and oxygen again a ring with melted and sintered ripples can be observed. For argon and nitrogen this ring almost vanishes and only little and weak ripples are present. For argon the crater is surrounded by

high amount of debris as expected from fig.4 whereas for nitrogen the debris near the crater does not significantly differ compared to oxygen and air. The changes due to nitrogen and oxygen in and around the craters obtained from an EDX analysis were too small for firmed statements.

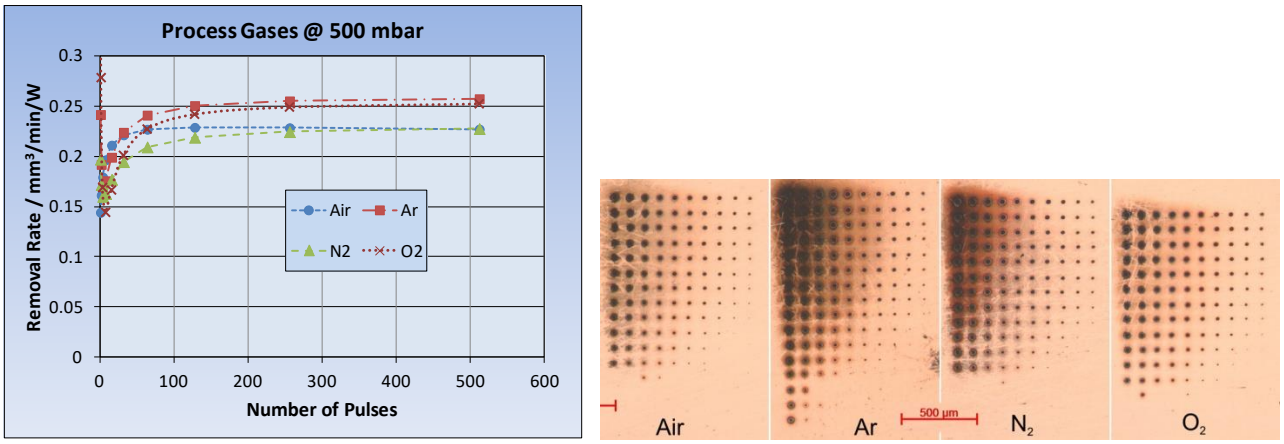

Figure 4. Left: Maximum removal rate for Cu-DHP calculated with the alternative model for 4 different process gases. Right: Ablated craters with raised pulse number from right to the left and decreased fluence top to down.

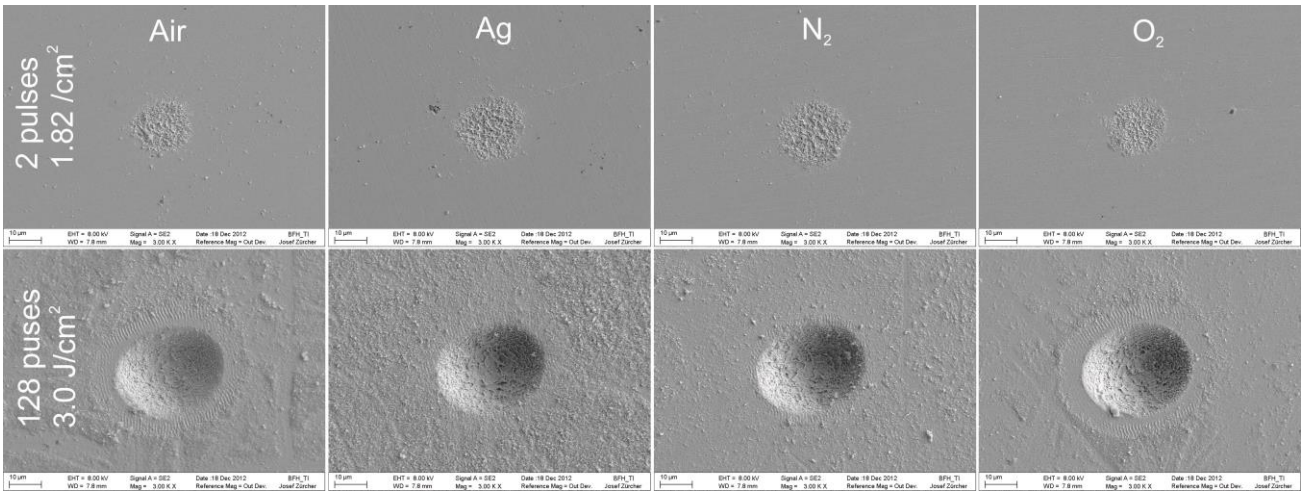

Figure 5. SEM pictures of ablated craters in Cu-DHP with 2 and 128 pulses at peak fluences of 1.82 J/cm^2 and 3.0 J/cm^2 in four different process gases and at a pressure of 500 mbar.

4.4 X-ray diffraction analysis

The strong dependence of the energy penetration on the number of pulses suggests that material changes could be responsible for the incubation. Therefore the series of ablated craters was machined in copper and iron single crystals with (111)-direction under a pressure 1 bar and 500mbar in sample one respectively 250mbar and 50 mbar in sample two. These samples were analyzed by HRXRD. Threshold fluence and penetration depth were measured for the series with 128 pulses under normal pressure, the values amounted $\phi_{th}=0.333J/cm^2\pm0.023J/cm^2$ and $\delta=44.5nm\pm1.8nm$ and are very close to the values measured for Cu-DHP ($\phi_{th}=0.350J/cm^2\pm0.008J/cm^2$ and $\delta=44.8nm\pm0.63nm$), i.e. the microstructure of Cu-DHP is assumed to be near a single crystal for small extension in the order of the spot diameter.

Figure 6 shows the HRXRD rocking curves of the two copper samples for a probe beam of 0.4x10mm extension. The curve width is correlated to the crystal tilt, the strain and the number of defects in the crystal lattice. The blue curves were taken in the untreated center of the samples and the red and green curves were measured in the irradiated areas. The curve widths did not vary significantly but a general observation is that broader peaks were observed in the platelets treated at lower pressures

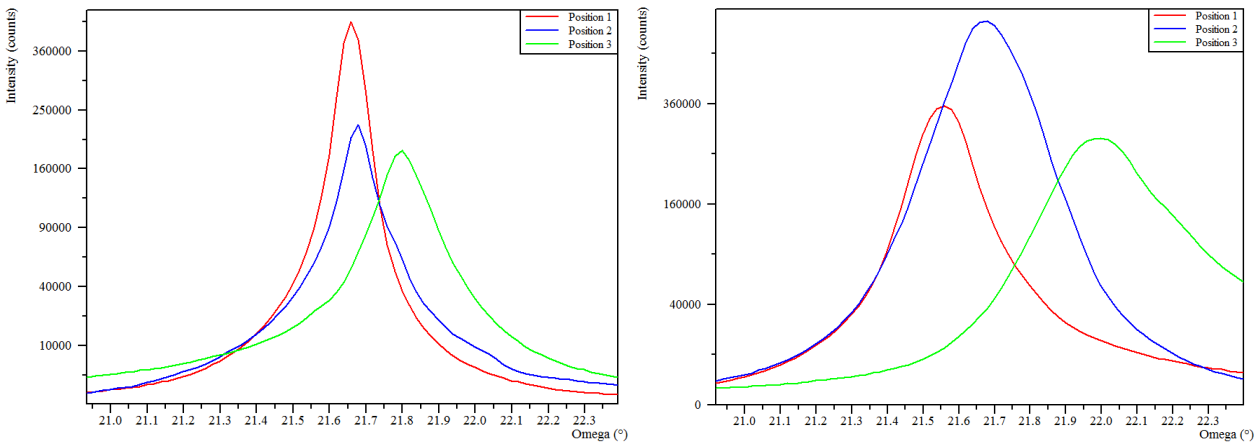

Figure 6. Rocking curves for the Cu sample 1 left and Cu sample 2 right. The blue curve indicates the spectrum of an untreated region (0.4x10mm) whereas the red curve is for normal pressure (left) respectively 250mbar pressure (right) and the green curve for 500mbar (left) and 50mbar (right).

Fig. 7 shows Reciprocal Space Maps (RSM) from a probe beam with 1x1mm dimension. Reciprocal space maps allow separating tilt, strain and diffuse scattering, which are superposed in the rocking curve scans. Structural defects would generate an increased incoherent part in the diffraction signal which would result in an increased background in the detected map. This is obviously not the case, i.e. no additional defects can be observed. Strains would lead to asymmetric peaks or streaks along the x-axis (Omega/2Theta-angle), which were also not observed.

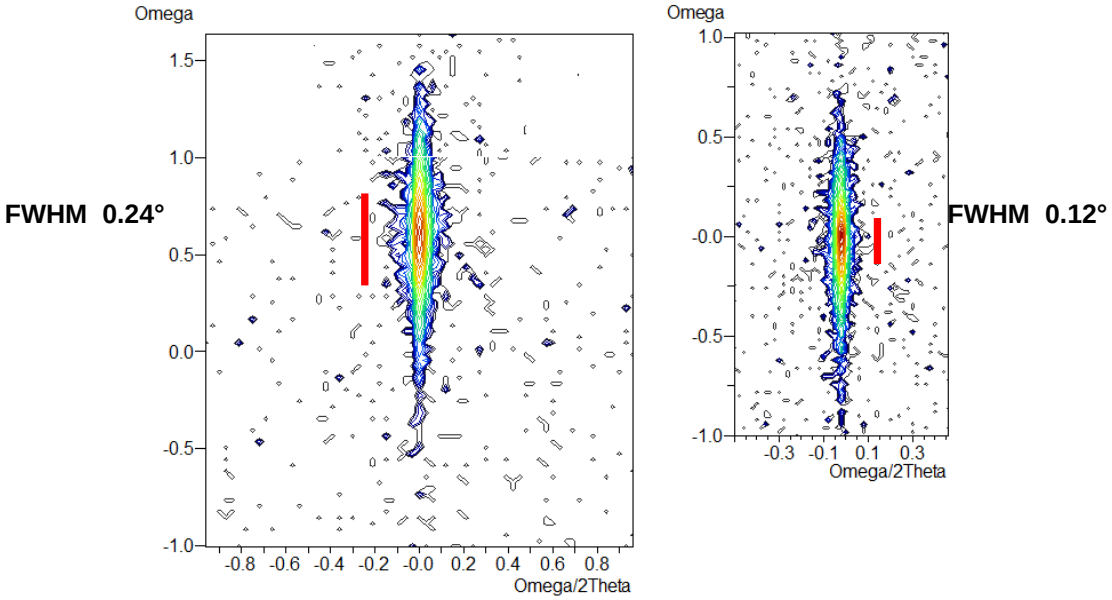

Figure 7. Reciprocal space maps from X-ray diffraction analysis of copper. Left: From a region treated at pressure of 50mbar on sample two. Right: From an untreated part on sample one.

The measurements of high resolution X-ray rocking curves and RSM's indicate that the peak broadening was mainly caused by crystal tilt and that the laser pulses did not induce significant changes in the strain state of the copper and iron crystals. A hypothesis is that this may be related to the formation of small-angle grain boundaries in the melted zones. The absence of strain and diffuse scattering suggests that the melted metal re-crystallizes into grains with low strain and defect levels. However, further investigations are required to clarify the processes on the micro-scale.

4.5 Reflectivity

Following (8) the reflectivity during the interaction of the laser pulses can be determined from the threshold fluence and the penetration depth as a function of the pulse duration under the assumption that the specific heat of evaporation Ω_{vap} is constant. The obtained values for the single- and infinite-pulse reflectivity are summarized in table 4.

All values are far below the normal Fresnel-reflectivity except the single-pulse reflectivity for iron. The values for copper deviate and show mean values of 0.41 ± 0.21 for single-pulse and 0.34 ± 0.09 for infinite-pulse reflectivity. The reduced reflectivity also reported by others[10] may be explained in different ways. First the formation of small surface ripples can increase the absorption[12]. For 2 pulses figs 3 and 5 show a significant increase of the surface roughness without considerable ablation which of course will reduce the reflectivity. A second reason could be the relaxation of optically excited electrons during the pulse[21]. A third possibility could be a different ablation process, especially for very short pulses, where it is assumed that clusters of the material are removed by a spallation process. This would reduce the energy needed for material removal and therefore increase the reflectivity following (8). However, additional measurements and investigations are needed to clarify the situation.

Table 4: Calculated single- and infinite- pulse reflectivity

Material/Gas	Cu/air	Cu/air	Cu/air	Cu/Ar	Cu/N_2	Cu/O_2	Al/air	Fe/air
p / mbar	1000	500	50	500	500	500	1000	1000
1 pulse	0.66	0.60	0.17	0.34	0.49	0.18	0.50	0.89
∞ pulses	0.45	0.41	0.29	0.20	0.37	0.32	0.32	0.24

5. CONCLUSION

The incubation was measured for a) Cu-DHP under different pressures and ambient gases and b) iron and aluminum under normal pressure an air. An alternative mathematical model is presented which better fits the high values of threshold fluence and penetration depth for low pulse numbers and eliminates the vanishing values for very high pulse numbers. It has been found that the incubation of the threshold fluence is mainly caused by a variation of the energy penetration depth which suggests that changes of material properties may be the driving factor. With X-ray diffraction analysis on (111) oriented copper and iron single crystals no significant increase of local defects in the crystal lattice were observed which is in conflict with explanations including thermal stress-strain energy storage cycles and accumulation of plastic deformations. However, more crystal tilt was observed which could be related to the formation of small-angle grain boundaries.

Further one finds that the removal rate depends on the surrounding pressure, e.g. a 25% increase was obtained when the pressure was reduced from normal condition down to 50mbar, but only marginal on the process gas.

Already for the first pulse the deduced reflectivity is below the Fresnel reflectivity which could be explained by optically excited electrons during the pulse or a different ablation process due to spallation. The decrease of the reflectivity for increasing pulse number can be explained by the increasing surface roughness.

But further investigations in different fields are required to gain more detailed insight into the nature of incubation.

6. ACKNOWLEGEMENTS

The authors wish to thank Josef Zuercher for his help with the SEM pictures. This work was supported by the Swiss Commission for Technology and Innovation CTI.

REFERENCES

[1] C. Momma, B.N. Chichkov, S. Nolte, F. van Alvensleben, A. Tünnermann, H. Welling and B. Wellegehausen, „Short-pulse laser ablation of solid targets,“ Opt. Comm. 129, 134-142 (1996)

[2] S. Nolte, C. Momma, H. Jacobs, A. Tünnermann, B.N. Chichkov, B. Wellegehausen and H. Welling, “Ablation of metals by ultrashort laser pulses,” J. Opt. Soc. Am. B, Vol. 14, No. 10 (1997)

[3] B. Neuenschwander, B. Jaeggi, M. Schmid, V. Rouffiange, P-E. Martin, " Optimization of the volume ablation rate for metals at different laser pulse-durations from ps to fs," Proceedings of SPIE vol. 8243, 824307-1 (2012)

[4] B. Neuenschwander, B. Jaeggi, M. Schmid, „From ps to fs: Dependence of the Material Removal Rate and the Surface Quality on the Pulse Duration for Metals, Semiconductors and Oxides," ICALEO 2012, Paper M1004, (2012)

[5] G. Mourou et al., "Method for controlling Configuration of laser induced breakdown and ablation," US Patent US RE37,585 E (2002)

[6] Y. Jee, M.F. Becker and R.M. Walser, "Laser-induced damage on single-crystal metal surfaces," J. Opt. Soc. Am. B5, (1988)

[7] C.S. Lee, N. Koumvakalis, M. Bass, „Spot-size dependence of laser induced damage to diamond-turned Cu-mirrors," Appl. Phys. Lett. 41, p. 625, 1982

[8] P.T. Mannion, J. Magee, E. Coyne, G.M. O'Connor, T.J. Glynn, "The effect of damage accumulation behavior on ablation thresholds and damage morphology in ultrafast laser micro-machining of common metals in air," Appl. Surf. Sci. 233, pp 275 – 287, 2004

[9] S.E. Kirkwood, A.C. Van Popta, Y.Y. Tsui, R. Fedosejevs, "Single and multiple shot near-infrared femtosecond laser pulse ablation thresholds of copper," Appl, Phys. A, 81, pp 729 – 735, 2005

[10] J. Byskov-Nielsen, J.M. Savolainen, M.S. Christensen, P. Balling, „Ultra-short pulse laser ablation of metals: threshold fluence, incubation coefficient and ablation rates," Appl. Phys. A, 101, pp 97 – 101, 2010

[11] J. Bonse, J.M. Wrobel, J. Krüger and W. Kautek, "Ultrashort-pulse laser ablation of indium phosphide in air," Appl. Phys. A; Vol. 72, 89 – 94 (2001)

[12] A. Rosenfeld, M. Lorenz, R. Stoian and D. Ashkenasi, "Ulrashort-laser-pulse damage threshold of transparent materials and the role of incubation," Appl. Phys. A; Vol. 69 [Suppl.], 373 – 376 (1999)

[13] M- Lenzer, J. Krueger, W. Kautek F. Krausz, „Incubation of laser ablation in fused silica with 5-fs pulses," Appl. Phys. A, 69, pp 456 – 466, 1999

[14] R. Lausten, J.A. Olesen, K. Vestentoft, P. Balling, „Ultrafast Phenomena XIII" Springer Series in Chemical Physics 71, p 675, 2002

[15] B. Neuenschwander, G. Bucher, G. Hennig, C. Nussbaum, B. Joss, M. Muralt, S. Zehnder et al., "Processing of dielectric materials and metals with ps laserpulses," ICALEO 2010, Paper M101

[16] B. N. Chichkov, C. Momma, S. Nolte, F. von Alvensleben and A. Tünnermann, „Femtosecond, picosecond and nanosecond laser ablation of solids," Appl. Phys. A 63, 109 (1996).

[17] C. Momma, S. Nolte, B.N. Chichkov, F. van Alvensleben and A. Tünnermann, "Precise laser ablation with ultrashort pulses," Appl. Surf. Science 109/110, 15-19 (1997)

[18] S.I. Anisimov and B. Rethfeld, "On the theory of ultrashort laser pulse interaction with a metal," Proc. SPIE 3093, 192-203 (1997)

[19] B.H. Christensen, K. Vestentoft and P. Balling, "Short-pulse ablation rates and the two-temperature model," Appl. Surf. Science 253, 6347-6352 (2007)

[20] P. Mannion, J. Magee. E. Coyne and G.M. O'Conner, "Ablation Thresholds in ultrafast laser micro-machining of common metals in air," Proc. of SPIE vol. 4876, 470-478 (2002)

[21] J. Hohlfeld, S.-S. Wellershoff, J. Güdde, U. Conrad, V. Jähnke, E. Matthias, „Electron and lattice dynamics following the optical excitation of metals," Chem. Phys. 251, pp. 237 – 258, 2000

[22] H. M. Urbasseka, Y. Rosandi, " Insight from molecular dynamics simulation into ultrashort-pulse laser ablation," Proc. of SPIE vol. 7842, 784214-1 – 784214-10, 2010